Journal of Mechanical Research and Application JMRA
ISSN: 2251-7383, eISSN: 2251-7391
Vol. 4, No. 2, 2012, 23-32

Stress Field Analysis of V-Notches with Tip Cracks in a Polymer Material Using Digital Image Correlation

N. Soltani[1], M. R. Yadegari[2*], I. Eshraghi[3]

Received: 2 Aug. 2012; Accepted: 12 Jan. 2013

Abstract: In this study, displacement field around v-notches of a poly methyl metha crylate (PMMA) specimen with tip cracks will be analyzed using digital image correlation technique. First intensity factor in combination with in-plane rigid body translations and rotation components will be determined by linear least squares fitting of the displacement field data to the corresponding relations among stress intensity factor and displacement field. The effect of v-notch angle on the results would be investigated. Experimental results will be compared with those obtained from finite element analysis. Good consistency is shown to exist between the results of two methods. The existence and a measure of a small region (corresponding to the plastic deformation zone in front of the crack tip) is demonstrated which should be excluded in data extraction for digital image correlation post-processing using linear elastic fracture mechanics relations.

Keywords: Digital Image Correlation, Fracture Mechanics, Least Squares, Stress Intensity Factor, V-Notch

1. Introduction

High stress concentrations at regions of structural discontinuity such as holes and notches may trigger initiation of cracks which, after a critical length is reached, may result in failure of whole or part of the structure. Thus it is necessary for designers to estimate critical length of the cracks and the crack growth rate. In this regard, determination of fracture parameters such as stress intensity factor or J integral is necessary for evaluating the strength and prediction of service life of engineering structures. Since analytical methods involve complicated calculations, non-contact and full-field measurement optics methods such as holographic interferometry, caustics, moiré interferometry and photoelasticity have been usually used for evaluation of fracture parameters [1, 2].

Among different techniques of full-field displacement measurement, digital image correlation (DIC) method has gained considerable attention during recent years because of its simplicity [3-5]. This method has become widely used mainly because it does not require complicated optical equipment. In contrast to most other optical methods, DIC is applicable to both opaque and transparent materials, and moreover the post-processing of images does not utilize fringe pattern analysis and phase-unwrapping [6]. Because of the mentioned convenience in using this method, many researchers applied it to various problems such as high temperature measurement [7], dynamic fracture [8] and submicron deformation measurement [9]. This method has also been used for determination of fracture parameters in various loading modes [10, 11]. To apply this method for determination of stress intensity factor, usually theoretical and experimental displacement fields in the local crack tip region are compared. Since this localized selection of displacement field data suffers from presence

1. Professor, School of Mechanical Engineering, College of Engineering University of Tehran, Tehran, Iran (nsoltani@ut.ac.ir)
2*. Corresponding Author: Center of Excellence in Intelligence- Based Experimental Mechanics, School of Mechanical Engineering, College of Engineering, University of Tehran, Tehran, Iran (m.yadegari@ut.ac.ir)
3. Ph. D. Student, Center of Excellence in Intelligence- Based Experimental Mechanics, School of Mechanical Engineering, College of Engineering University of Tehran, Tehran, Iran (ieshraghi@ut.ac.ir)

of errors in the experimental data, it has been suggested that full-field information may be used to eliminate these errors [8].

The usual application of DIC, using linear elastic fracture mechanics (LEFM) is that experimental displacement field data in the local crack tip region are substituted in appropriate analytical relations, which relate fracture parameters to displacement components. The corresponding least squares problem is solved to determine unknown parameters such as stress intensity factors and rigid body displacements and rotations [12]. However, application of LEFM relations for determination of displacement components imposes restrictions on the selection of data-points extraction region for DIC analysis. This is mainly due to formation of small plastic zone in front of the crack tips in which LEFM stress-displacement relations are no longer valid. Most studies [11, 12] which concern with the determination of SIFs use suggested theoretical values [13] for this radius and exclude data points located in this area from their analysis. However the effect of this parameter on the calculated SIFs has been rarely investigated by researchers.

In this study, displacement field obtained from DIC experiment have been used to determine stress intensity factor for mode-I fracture problem of a PMMA sample. Linear least-squares approach is applied to obtain unknowns such as stress intensity factors and rigid body displacements and rotation. The effects of v-notch opening angle is investigated and compared to those obtained by finite element (FE) analysis. In order to examine the properness of using LEFM relations in studying fracture parameters of a PMMA sample, effects of minimum radius of data-points extraction zone on the accuracy and convergence of the results of first intensity factor has also been investigated.

2. DIC basics and experimental setup

2.1. Fundamentals of digital image correlation

In general, three consecutive steps are included in two dimensional DIC method. These steps are namely (1) preparation of specimen and experimental system; (2) recording images of the planar specimen surface before and after loading; (3) utilizing a computer program for post processing of the acquired images to obtain displacement and strain field information. To perform the first step, a random speckle-like black and white dot patterns are created on specimen surfaces. For the next step the camera is placed with its optical axis normal to the specimen surface, imaging the planar specimen surface in different loading states onto its sensor plane. The digitized images are compared and subsets are matched between one image and the other to finalize the required steps of performing a DIC technique. A subset may comprise several pixels depending on the choice of the loading and required accuracy. Then its location in the deformed image is found and thus its displacements are determined. A normalized cross-correlation coefficient, C, defined by the Eq. (1) is used to improve the estimate of the displacements [5, 10].

$$C\left(x, y, u, v, \frac{\partial u}{\partial x}, \frac{\partial u}{\partial y}, \frac{\partial v}{\partial x}, \frac{\partial v}{\partial y}\right) = 1 - \frac{\sum G_r(x, y) G_d(x', y')}{\sqrt{\sum G_r(x, y)^2 G_d(x', y')^2}} \tag{1}$$

where (x, y) are the location of any point in the subset before deformation and the following terms in parentheses in the LHS of Eq. (1) represent displacements and displacements gradients in x and y directions at the center of the subset. G_r and G_d are the grey levels of the reference and deformed images, respectively, and (x', y') are the coordinates of the point (x, y) in the subset after deformation as shown in Fig. 1. (x', y') is related to (x, y) by Eq. (2):

$$\begin{aligned} x' &= x + u + \frac{\partial u}{\partial x}\Delta x + \frac{\partial u}{\partial y}\Delta y, \\ y' &= y + v + \frac{\partial v}{\partial x}\Delta x + \frac{\partial v}{\partial y}\Delta y, \end{aligned} \tag{2}$$

in which Δx and Δy are distances from the subset center to the point (x, y) in the x and y directions respectively. Since the correlation coefficient C is a function of the displacement and displacement gradients components, these components are determined by looking for a set of the displacements and

a set of displacement gradients that minimize this correlation coefficient. The displacements in Eq. (2) can take sub-pixel values, so an interpolation scheme must be employed to determine the intensity values at sub-pixel locations. Two major interpolation schemes are bilinear and bicubic interpolations. The bilinear interpolation scheme could be described by Eq. (3) given by:

$$G_d(x', y') = a_{00} + (a_{10} - a_{00})\Delta x^* + (a_{01} - a_{00})\Delta y^* + (a_{11} + a_{00} - a_{01} - a_{10})\Delta x^* \Delta y^* \quad (3)$$

where

a_{00} is the intensity value of pixel *(i,j)*

a_{10} is the intensity value of pixel *(i+1,j)*

a_{01} is the intensity value of pixel *(i,j+1)*

a_{11} is the intensity value of pixel *(i+1,j+1)*

Δx^* and Δy^* are the relative distances of the point from pixel *(i,j)*.The process of searching for unknown displacement and displacement gradients components begins with a rough estimate of displacement components and setting displacement gradients equal to zero. At the end of this step the displacements are found with an accuracy of 1 pixel. Then Newton-Raphson method is then used to find displacement gradients and displacement components with sub-pixel accuracy. The results of previous step are considered as the initial values for the Newton-Raphson method. More details can be found in the works by Bruck et al. [5] and Lu and Cary [14].

2.2. Estimation of stress intensity factor

Considering mode-I loading condition of cracks in plane problem, the displacement fields around a crack tip (taking in to account only the first term of the expressions) are expressed by Eq. (4) as:

$$u = \frac{K_I}{\sqrt{2\pi}} \frac{\sqrt{r}}{2\mu} \left[\left(\kappa - \frac{1}{2} \right) \cos\frac{\theta}{2} - \frac{1}{2} \cos\frac{3\theta}{2} \right],$$
$$v = \frac{K_I}{\sqrt{2\pi}} \frac{\sqrt{r}}{2\mu} \left[\left(\kappa + \frac{1}{2} \right) \sin\frac{\theta}{2} - \frac{1}{2} \sin\frac{3\theta}{2} \right]. \quad (4)$$

where u and v are the displacement components, μ is the shear modulus, and κ is $(3-\nu)/(1+\nu)$ for plane stress and $3-4\nu$ for plane strain. r and θ are the polar coordinates of a pint relative to the crack tip location as shown in Fig. 2.

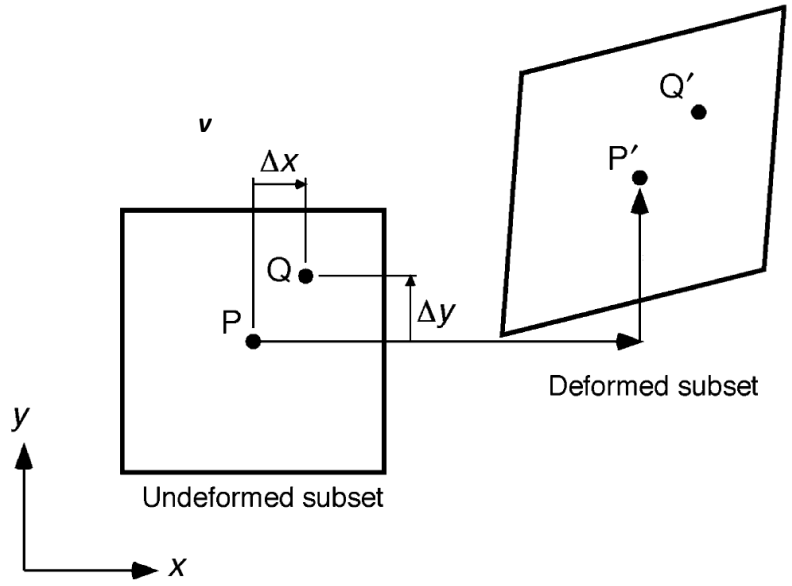

Fig. 1. Undefomed and deformed subsets [6].

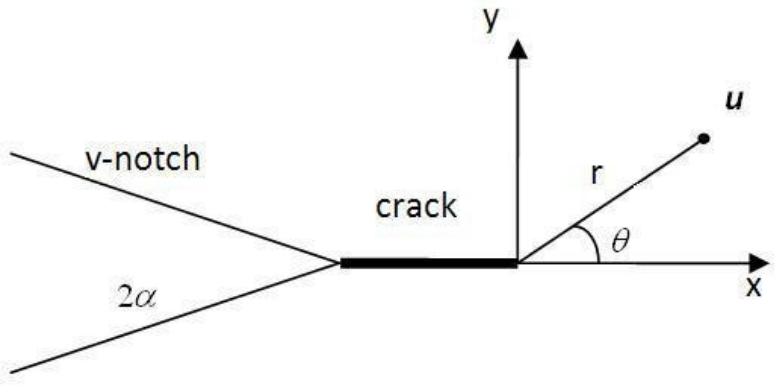

Fig. 2. Cartesian and polar coordinates at the crack tip of a v-notch.

For a displacement data point taking into account in-plane rigid body displacements and rigid body rotation the displacement components can be re-written as given in Eq. (5):

$$u_j = \frac{K_I}{\sqrt{2\pi}} \frac{\sqrt{r_j}}{2\mu}\left[\left(\kappa - \frac{1}{2}\right)\cos\frac{\theta_j}{2} - \frac{1}{2}\cos\frac{3\theta_j}{2}\right] + u_0 - \varphi r_j \sin\theta_j,$$

$$v = \frac{K_I}{\sqrt{2\pi}} \frac{\sqrt{r_j}}{2\mu}\left[\left(\kappa + \frac{1}{2}\right)\sin\frac{\theta_j}{2} - \frac{1}{2}\sin\frac{3\theta_j}{2}\right] + v_0 + \varphi r_j \cos\theta_j. \quad (5)$$

Where u_0 and v_0 are the rigid body displacement components and φ is the rigid body rotation angle in radians. The Subscript j denotes the *j*th data point with the coordinate (x_j, y_j) of M total data points. Polar coordinates (r_j, θ_j) are related to Cartesian coordinates (x_j, y_j) by Eq. (6):

$$r_j = \sqrt{(x_j - x_0)^2 + (y_j - y_0)^2},$$
$$\theta_j = \tan^{-1}\frac{(y_j - y_0)}{(x_j - x_0)}. \quad (6)$$

where (x_0, y_0) is the Cartesian coordinates of crack tip location. The location of the crack tip is to be determined through precise inspection of the images. Here linear least square fitting will be used to evaluate unknowns K_I, u_0, v_0 and φ.

2.3. Specimens and test setup

PMMA was used as the test material. Elasticity modulus E and Poisson's ratio ν of the material were measured to be as E=3.33 GPa and $\nu = 0.33$ respectively. The specimen and the experimental setup are shown in Fig. 3. The width of the specimen is 50 mm and its thickness is equal to 4 mm. DIC tests were performed for four different notch angles of magnitude $2\alpha = 30°, 60°, 90°, 120°$. For the purpose of determining the magnification factor and subset size, rigid body translation tests were performed. The magnitude of the applied axial force was varied from 0 to 70 kgf with a step of 3.5 kgf. Random patterns on the specimen surface were recorded by a charged-coupled device (CCD) camera (Art-Cam 320p equipped with a Fujian 55 mm lens). The images were captured with a spatial resolution of 2288×1700 pixels. A servo control system universal testing machine (AI-7000-S GOTECH testing Machines Inc.) with 20 kN capacity has been used for applying mode-I fracture loading conditions on the specimen. The DIC optical setup was settled on a vibration isolated table in order to eliminate noises. Each 1 mm of real distance corresponds to 20.41 pixels in the scaled images used for analysis. The experimental setup system is shown in Fig. 3.

3. Finite element modeling

For the purpose of comparison a finite element model has been created for analyzing the stress intensity factor of the specimen under given applied load. Fig. 4 shows the FE model and type of mesh used in the vicinity of the crack tip. Because of symmetry, only half of the specimen has been modeled with symmetric boundary conditions applied on the lower line of the model. A constant distributed tensile load of magnitude 70 kgf $\times$ 4 mm

Fig. 3. Experimental setup.

has been applied to upper edge of the model. Five contours were taken around crack tip for estimation of the crack intensity factor. The magnitude of stress intensity factor is computed for a load step of 3.5 kgf which corresponds to that of experimental data.

4. Results and discussion

To investigate the convergence behavior of the results with the distance from the crack tip, non-dimensional stress intensity factors for various v-notch angles are plotted against the distance from crack tip in Fig. 5. Non-dimensional stress intensity factor is defined as $K_I^* = \frac{K_I}{\sigma_\infty W}$ where σ_∞ is the far field stress and W is the width of the specimen. As it may be seen for this specific type of geometry, notch angle has negligible effect on stress intensity factors and the results are converged after a sufficient distance from crack tip. This distance may properly be referenced to the small plastic deformation zone in front of the crack tip. Using the material points located in this region in DIC post-processing analysis invalidates utilizing LEFM relations in least-squares fitting. The proper determination of the radius of this region has substantial effect on the accuracy of calculated results for stress intensity factor. For the case considered here (a PMMA sample in mode-I fracture loading conditions), a 6 mm distance is sufficient in obtaining converged and accurate results. Fig. 6 indicates the relative difference of the results for various v-notch angles with the stress intensity factor obtained for a 120° v-notch angle. The maximum relative difference present in the results is about 6.5% for converged values. The effect of minimum radius of data extraction zone for different v-notch angles may be observed from this figure.

Results of displacement fields obtained from a DIC analysis of a specimen with a 30° v-notch angle are shown in Fig. 7. 50 data points are extracted from the obtained displacement fields to perform a least square fitting for determining the stress intensity factor. The magnitude of the standard error and correlation coefficient (for least square fitting) are equal to 3e-7 and 0.97 respectively for the applied load of 70 kgf. The magnitude of obtained stress intensity factor from DIC analysis and FE modeling for various loads and various v-notch angles are given in Fig. 8 (a) to (d). These figures show good agreement between the results of finite element analysis and DIC experiment. Deformation of the FE model after applying the tensile load in combination with the crack opening is also shown in Fig. 9. The maximum error between the results is 8% for 90° v-notch angle and for a load of 31.5 kgf. As it may be observed the magnitude of v-notch angle has negligible effect on the values of stress intensity factor. Also it may be noticed that the percentage of the error for experimental data decreases with increase of the applied load. This is mainly because higher axial loads produce greater displacements which will result in relatively smaller errors in estimation of the displacement fields during DIC post processing. The linear variation of first intensity factor with the applied load is also clear from the given figures for both of FE and DIC results for all v-notch angles.

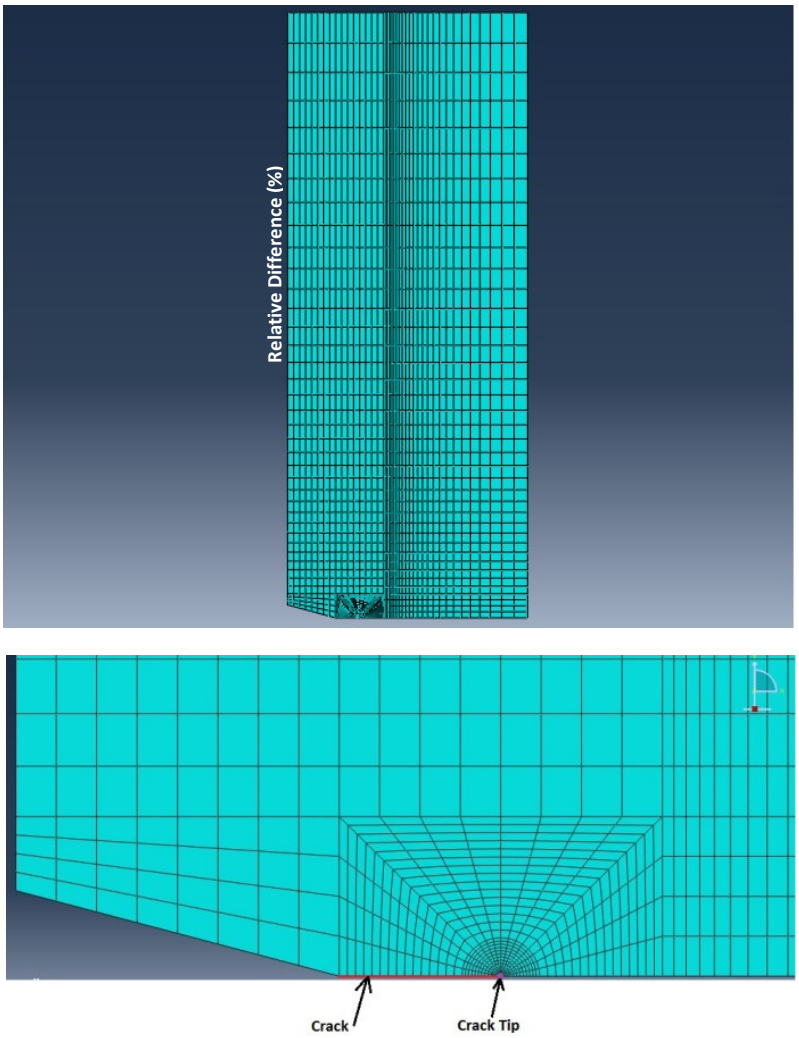

Fig. 4. Finite element model (up) and the mesh around the crack (down).

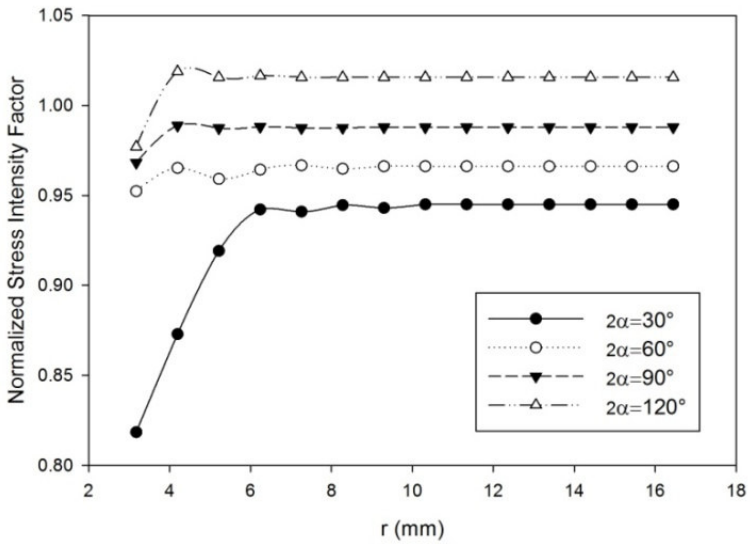

Fig. 5. Convergence behavior of the stress intensity factor results with the distance from crack tip for various v-notch angles.

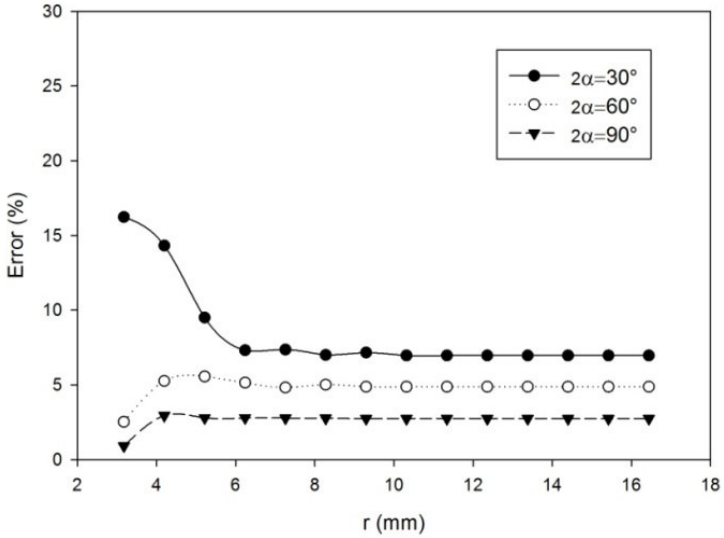

Fig. 6. Comparison of the relative difference in the stress intensity factor obtained for various v-notch angles in comparison with 120° v-notch angle result.

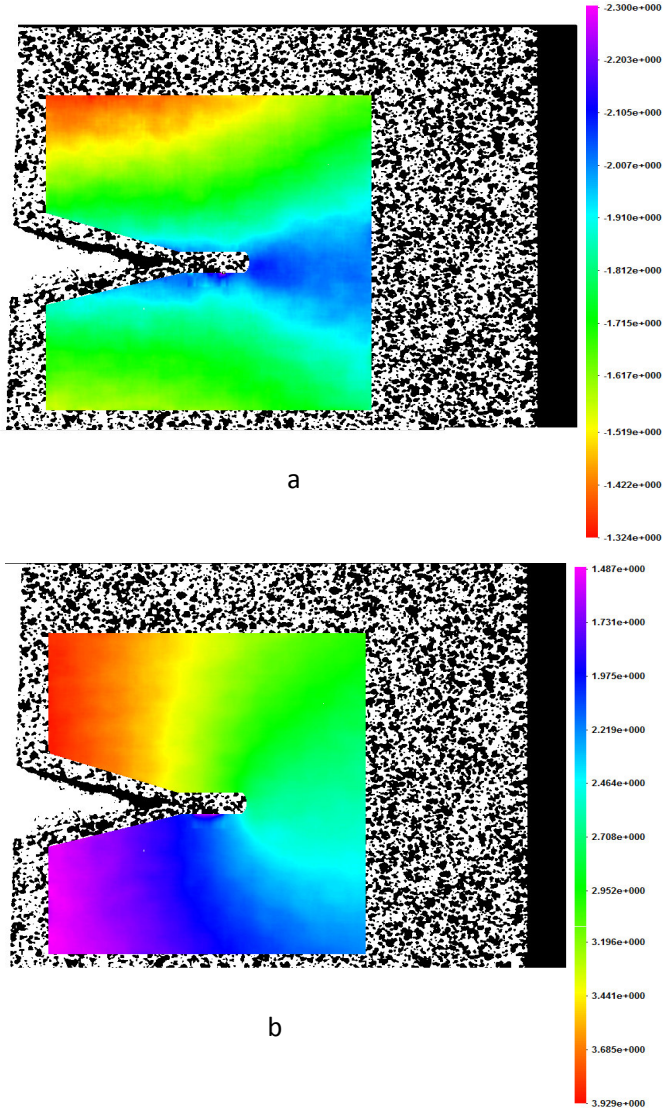

Fig. 7. Displacement field obtained from DIC experiment: (a) displacement field in x direction (b) displacement field in y direction.

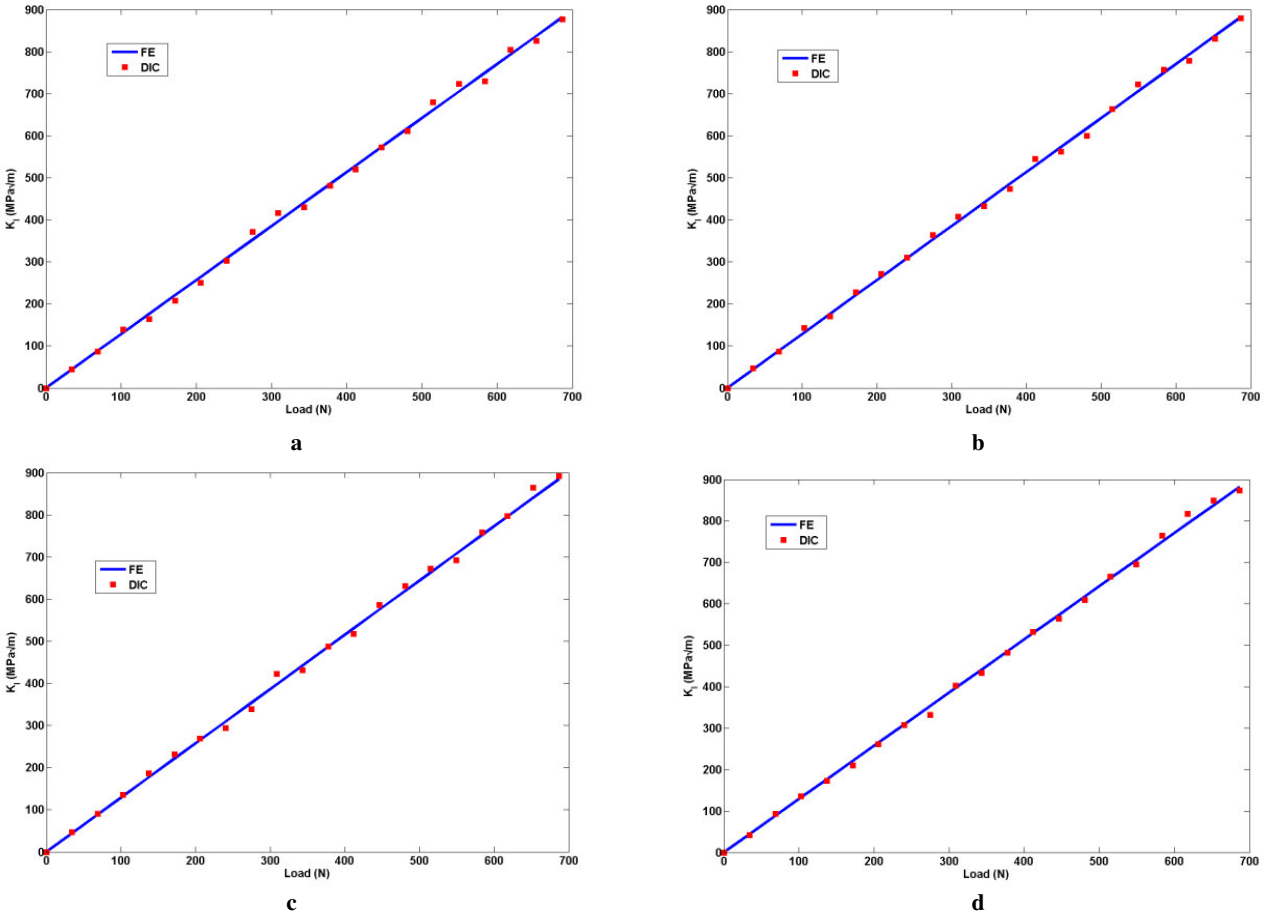

Fig. 8. Variation of first intensity factor with the applied load for various v-notch angles and obtained from finite element and DIC analysis. (a) $2\alpha = 30^\circ$ **(b)** $2\alpha = 60^\circ$ **(c)** $2\alpha = 90^\circ$ **(d)** $2\alpha = 120^\circ$

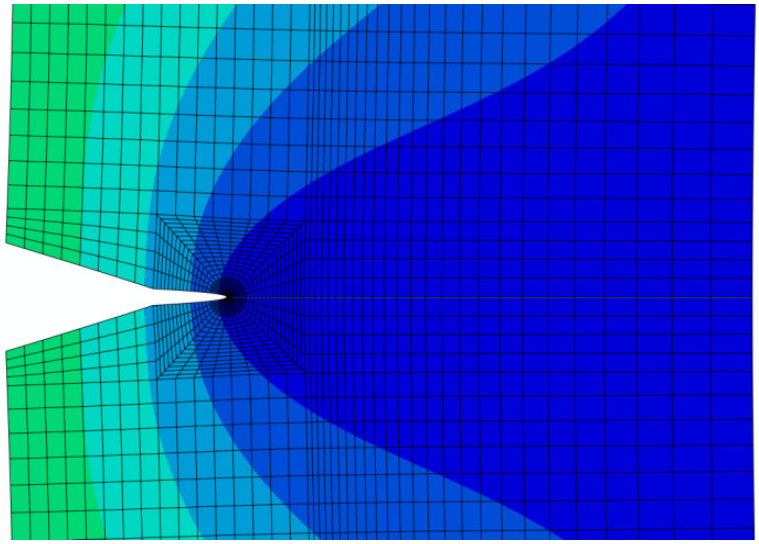

Fig. 9. Opening of the crack after loading in FE model.

5. Conclusions

An experimental study was performed to determine first stress intensity factor of a PMMA specimen under mode-I loading condition. Since linear elastic fracture mechanics relations were used to correlate experimental displacement field and fracture parameters, effect of radius of data extraction zone in front of crack on the convergence and accuracy of the results was investigated. It was shown that that for the case considered in this study there is a minimum distance (corresponding to local region of plastic deformation in front of the crack tip location) that should be excluded from DIC data post-processing analysis. The minimum radius was determined to be 6mm for the PMMA sample considered with specified geometric parameters. It was also shown that the magnitude of v-notch angle has negligible effect on this radius.

Results of DIC analysis were compared to those given by finite element analysis and excellent agreement was shown to exist. Maximum percentage error was 6% for lower values of applied load while this value decreases to 3% for higher load magnitudes. It was also shown that the v-notch angle has negligible effect on the value of first intensity factor when the length of crack is held constant. Linearity of the first intensity factor with applied load was also observed in the case of a v-notch with a tip crack within the elastic region and for mode-I loading conditions.

Nomenclature

r	Distance from crack tip
u, v	Displacement components in x and y directions
u_0, v_0	Rigid body translations in x and y directions
C	Cross correlation coefficient
G_d, G_r	Grey levels of deformed and reference images respectively
K_I	First intensity factor ($MPa\sqrt{m}$)
α	v-notch half angle
κ	Plane strain or plane stress determining parameter
μ	Shear modulus (MPa)
υ	Poisson's ratio
φ	Rigid body rotation angle (*rad*)

References

[1] Smith C. W. and Kobayashi A. S., "Experimental fracture mechanics," in Handbook on Experimental Mechanics, Kobayashi A. S., ed. (VCH, New York, 1993), pp. 905-968.

[2] Chiang F., "Moire´ and speckle methods applied to elastic-plastic fracture studies." in Experimental Techniques in Fracture Mechanics, Epstein J. S., ed. (VCH, New York, 1993), pp. 291-325.

[3] Peters W. H. and Ranson W. F., "Digital imaging technique in experimental stress analysis," Optical Engineering, 1982; 21: 427-431.

[4] Sutton M. A, Wolters W. J., Peters W. H., Ranson W. F. and McNeill S. R., "Determination of displacements using an improved digital correlation method," Image and Vision Computing, 1983; 1: 133-139.

[5] Bruck H. A., McNeill S. R., Sutton M. A. and Peters W.H., "Digital image correlation using Newton-Raphson method of partial differential correlation," Experimental Mechanics, 1989; 29: 261–268.

[6] Yoneyama S., Morimoto Y., and Takashi M., "Automatic evaluation of mixed-mode stress intensity factors utilizing digital image correlation", Strain, 2006; 42: 21-29.

[7] Lyons J. S., Liu J., Sutton M. A.," High-temperature deformation measurements using digital-image correlation", Experimental Mechanics, 1996; 36(1): 64-70.

[8] Andanto-Bueno J. and Lambros J., "Investigation of crack growth in functionally graded materials using digital image correlation," Engineering Fracture Mechanics, 2002; 69: 1695-1711.

[9] Vendroux G. and Knauss W. G., "Submicron deformation field measurements: part 2. Improved digital image correlation," Experimental Mechanics, 1998; 38: 86-92.

[10] McNeill S. R., Peters W. H., and Sutton M. A., "Estimation of stress intensity factor by digital image correlation," Engineering Fracture Mechanics, 1987; 28: 101-112.

[11] S. Yoneyama, T. Ogawa , Y. Kobayashi, "Evaluating mixed-mode stress intensity factors from full-field displacement fields obtained by optical methods", Engineering Fracture Mechanics, 2007; 74: 1399–1412.

[12] Rui Zhangn , Lingfeng He, "Measurement of mixed-mode stress intensity factors using digital image correlation method", Optics and Lasers in Engineering, 2012; 50: 1001-1007.

[13] Gdoutos E.E. 2nd ed. Fracture Mechanics: an introduction, 18. Springer; 2005.

[14] Lu, H. M. and Cary, P. D., "Deformation measurements by digital image correlation: Implementation of a second-order displacement gradient," Journal of Experimental Mechanics, 2000; 40 (4): 393–400.